

Maximum Likelihood Estimation of the Non-Parametric FRF for Pulse-Like Excitations

Roland Hostettler, Wolfgang Birk, and Magnus Lundberg Nordenvaad

This is a post-print of a paper published in *IEEE Transactions on Automatic Control*. When citing this work, you must always cite the original article:

R. Hostettler, W. Birk, and M. Lundberg Nordenvaad, "Maximum likelihood estimation of the non-parametric FRF for pulse-like excitations," *Automatic Control, IEEE Transactions on*, vol. 61, no. 8, pp. 2276–2281, August 2016

DOI

10.1109/TAC.2015.2491538

Copyright

© 2016 IEEE. Personal use of this material is permitted. Permission from IEEE must be obtained for all other uses, in any current or future media, including reprinting/republishing this material for advertising or promotional purposes, creating new collective works, for resale or redistribution to servers or lists, or reuse of any copyrighted component of this work in other works.

Maximum Likelihood Estimation of the Non-Parametric FRF for Pulse-Like Excitations

Roland Hostettler, *Member, IEEE*, Wolfgang Birk, *Member, IEEE*, Magnus Lundberg Nordenvaad

Abstract—This paper introduces the closed form maximum likelihood estimator for estimating the coefficients of the non-parametric frequency response function from system identification experiments. It is assumed that the experiments consist of repeated pulse excitations and that both the excitation and system response are measured which leads to an error-in-variables setting. Monte Carlo simulations indicate that the estimator achieves efficiency at low signal-to-noise ratios with only few measurements. Comparison with the least-squares estimator shows that better, unbiased results are obtained.

Index Terms—System Identification, Linear Systems, Maximum Likelihood Estimation

I. INTRODUCTION

System identification for linear systems is an important and well-established topic within different engineering fields such as control engineering. It is often used as a tool for gaining insight into the dynamic properties of a system under consideration or for model building, for example for automatic control applications. Thus, it is not surprising that the field has had a great deal of attention from the research community during the last decades. Standard textbooks such as [1] and [2] give thorough introductions from experiment design to measurement data analysis. It is well understood that in order to gain as much insight as possible a system should be excited in a broad frequency range. The excitation signals best suited for this purpose are white Gaussian random noise or random phase multisines [3] since these two types have the desired broadband properties. Random phase multisines are especially useful since the user can carefully choose parameters such as bandwidth and excitation frequencies. Furthermore, multisines are very well suited for detecting nonlinearities in the system [3].

Nevertheless, there are sometimes situations where the practitioner is limited in how the system can be excited and has to resort to alternative approaches since it might be impractical to apply an ideal excitation due to equipment or other limitations. It is thus not uncommon to apply simple excitations such as pulses or other non-random excitations instead. Typical applications include the evaluation of mechanical structures or the response of a biological system to drug intake. Obviously, this also imposes certain limitations to the amount of information that can be obtained but nevertheless this approach might be the only alternative.

When such an approach is used, it is often the case that both the excitation as well as the system response have to be measured and thus, both the input and output measurements are noisy which leads to an error-in-variables setting. While there is a well established knowledge about how to estimate non-parametric as well as parametric frequency response functions (FRF) when using random noise or random phase multisine excitation signals [4]-[6], the analysis of repeated, possibly non-reproducible, pulse excitation experiments has gained a lot less attention within the system identification literature, possibly due to the apparent drawbacks of the excitation signal. However, the problem is closely related to the problem of linear regression where both variables are subject to noise, see [7] for a quick overview. Further, a method for estimating parametric FRFs

R. Hostettler and W. Birk are with the Division of Signals and Systems, Luleå University of Technology, Luleå, Sweden.

M. Lundberg Nordenvaad is with the Swedish Defense Research Agency (FOI), Stockholm, Sweden.

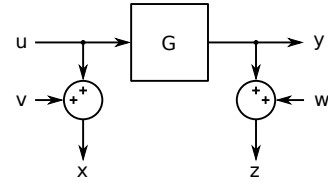


Fig. 1. Error-in-variables system identification setting. The true input signal $u(t)$ and output signal $y(t)$ are measured as noise-corrupted versions $x(t)$ and $z(t)$, respectively. The measurement noises are $v(t)$ and $w(t)$.

from a single error-in-variables experiment with non-white input was proposed in [8].

It is the aim of this technical note to consider system identification experiments under the circumstances mentioned above. Specifically, the contribution of this technical note is the hitherto unknown closed form maximum likelihood estimator for the non-parametric FRF under the following assumptions:

- The measurement data consists of a set of $m = 1, \dots, M$ non-random and periodic (with respect to the measurement window) input-output signal pairs.
- The input-output measurements are both corrupted by measurement noise.
- The excitation signal may vary between each repetition, that is, be non-reproducible.

Note that while this problem seems to be of general interest, it has not yet been treated in the literature.

The estimator is derived in Section II and numerically illustrated in Section III. Some concluding remarks are given in Section IV.

II. THEORY

Consider the error-in-variables setting as illustrated in Fig. 1 and assume that a total of M independent experiments are performed where the input signals are pulses and the true excitations $u_1(t) \neq u_2(t) \neq \dots \neq u_M(t)$ are different for each experiment. Furthermore, both the input signal $u_m(t)$ and output $y_m(t)$ are disturbed by noise. The measured input- and output signals can then be modeled as

$$\begin{aligned} x_m(n) &= u_m(n) + v(n) \\ z_m(n) &= y_m(n) + w(n) \\ &= g(n) * u_m(n) + w(n) \end{aligned} \quad (1)$$

where the continuous signal is sampled at $t = nT_s$, $g(n)$ denotes the pulse response of the system, and $*$ the convolution. The additive noise is assumed to capture effects like thermal noise and other disturbances in the measurement equipment and is assumed to be white Gaussian noise of the form $v(n) \sim \mathcal{N}(0, \sigma_v^2)$ and $w(n) \sim \mathcal{N}(0, \sigma_w^2)$, and mutually uncorrelated, that is, $E\{v(n)w(n)\} = 0$.

Granted that both the input and output have decayed to zero the unitary discrete Fourier transform of (1) yields

$$\begin{aligned} X_m(\omega_l) &= U_m(\omega_l) + V(\omega_l) \\ Z_m(\omega_l) &= G(\omega_l)U_m(\omega_l) + W(\omega_l) \end{aligned} \quad (2)$$

for $l = 1, \dots, N/2 - 1$ where

$$\omega_l = \frac{2\pi f_s l}{N},$$

$f_s = 1/T_s$ is the sampling frequency and N the number of samples. Note that if it is ensured that the complete finite-time sequences $x_m(n)$ and $y_m(n)$ are measured from rest to rest, leakage errors can be avoided. However, the finite time pulse will have an infinite spectrum and hence, aliasing problems may occur if the pulse duration is chosen badly in relation to the sampling frequency.

The noise components $V(\omega_l)$ and $W(\omega_l)$ in (2) are circular, complex normal distributed [9] according to

$$V(\omega_l) \sim \mathcal{CN}(0, \sigma_v^2) \quad \text{and} \quad W(\omega_l) \sim \mathcal{CN}(0, \sigma_w^2)$$

For each frequency ω_l (ω_l will be dropped for the remainder of the paper) we are now given $2M$ measurement samples X_1, \dots, X_M and Z_1, \dots, Z_M and $M+1$ unknowns

$$\boldsymbol{\theta} = [U_1 \quad \dots \quad U_M \quad G]^T.$$

In order to estimate the non-parametric FRF, it is mainly the Fourier coefficient G that is of interest. Letting

$$\begin{aligned} \mathbf{U} &= [U_1 \quad \dots \quad U_M]^T, \\ \mathbf{X} &= [X_1 \quad \dots \quad X_M]^T, \\ \mathbf{Z} &= [Z_1 \quad \dots \quad Z_M]^T, \end{aligned}$$

the joint probability density function (PDF) is given by

$$\begin{aligned} p(\mathbf{X}, \mathbf{Z}; \boldsymbol{\theta}) &= \mathcal{CN} \left(\begin{bmatrix} \mathbf{X} \\ \mathbf{Z} \end{bmatrix}; \begin{bmatrix} \mathbf{U} \\ G\mathbf{U} \end{bmatrix}, \begin{bmatrix} \sigma_v^2 \mathbf{I}_M & \mathbf{0} \\ \mathbf{0} & \sigma_w^2 \mathbf{I}_M \end{bmatrix} \right) \\ &= \mathcal{CN} \left(\begin{bmatrix} \mathbf{X} \\ \mathbf{Z} \end{bmatrix}; \mathbf{H}\mathbf{U}, \mathbf{C} \right) \end{aligned} \quad (3)$$

with

$$\mathbf{H} = \begin{bmatrix} \mathbf{I}_M \\ G\mathbf{I}_M \end{bmatrix} \quad \text{and} \quad \mathbf{C} = \begin{bmatrix} \sigma_v^2 \mathbf{I}_M & \mathbf{0} \\ \mathbf{0} & \sigma_w^2 \mathbf{I}_M \end{bmatrix}$$

and \mathbf{I}_M the $M \times M$ identity matrix.

The maximum likelihood estimator (MLE) for $\boldsymbol{\theta}$ is then given by [9]

$$\hat{\boldsymbol{\theta}} = \underset{\boldsymbol{\theta}}{\operatorname{argmax}} - \left(\begin{bmatrix} \mathbf{X} \\ \mathbf{Z} \end{bmatrix} - \mathbf{H}\mathbf{U} \right)^H \mathbf{C}^{-1} \left(\begin{bmatrix} \mathbf{X} \\ \mathbf{Z} \end{bmatrix} - \mathbf{H}\mathbf{U} \right)$$

where the superscript H denotes the conjugate transpose. Since the mean of (3) is linear in \mathbf{U} the problem is separable. This in turn means that the ML estimate \hat{G} is found by maximizing the cost [9]

$$\begin{aligned} J(G) &= \begin{bmatrix} \mathbf{X} \\ \mathbf{Z} \end{bmatrix}^H \mathbf{C}^{-1} \mathbf{H} \left(\mathbf{H}^H \mathbf{C}^{-1} \mathbf{H} \right)^{-1} \mathbf{H}^H \mathbf{C}^{-1} \begin{bmatrix} \mathbf{X} \\ \mathbf{Z} \end{bmatrix} \\ &= \left(\frac{\mathbf{X}}{\sigma_v^2} + \frac{G^* \mathbf{Z}}{\sigma_w^2} \right)^H \left(\frac{\mathbf{X}}{\sigma_v^2} + \frac{G^* \mathbf{Z}}{\sigma_w^2} \right) \left(\frac{1}{\sigma_v^2} + \frac{GG^*}{\sigma_w^2} \right)^{-1} \\ &= \left(\frac{\mathbf{X}^H \mathbf{X}}{(\sigma_v^2)^2} + \frac{G^* \mathbf{X}^H \mathbf{Z} + G \mathbf{Z}^H \mathbf{X}}{\sigma_v^2 \sigma_w^2} + \frac{GG^* \mathbf{Z}^H \mathbf{Z}}{(\sigma_w^2)^2} \right) \\ &\quad \times \left(\frac{1}{\sigma_v^2} + \frac{GG^*}{\sigma_w^2} \right)^{-1}. \end{aligned} \quad (4)$$

The stationary points for (4) are found by setting the derivative $\partial J(G)/\partial G^* = 0$ where the derivative with respect to a complex variable is defined as in [10] and the superscript $*$ denotes the complex conjugate. Then, (4) becomes

$$\begin{aligned} \frac{\partial J(G)}{\partial G^*} &= \left(\frac{1}{\sigma_v^2} + \frac{GG^*}{\sigma_w^2} \right)^{-1} \left(\frac{\mathbf{X}^H \mathbf{Z}}{\sigma_v^2 \sigma_w^2} + \frac{G \mathbf{Z}^H \mathbf{Z}}{(\sigma_w^2)^2} \right) \\ &\quad - \frac{G}{\sigma_w^2} \left(\frac{1}{\sigma_v^2} + \frac{GG^*}{\sigma_w^2} \right)^{-2} \\ &\quad \times \left(\frac{\mathbf{X}^H \mathbf{X}}{(\sigma_v^2)^2} + \frac{G^* \mathbf{X}^H \mathbf{Z} + G \mathbf{Z}^H \mathbf{X}}{\sigma_v^2 \sigma_w^2} + \frac{GG^* \mathbf{Z}^H \mathbf{Z}}{(\sigma_w^2)^2} \right) \\ &= 0 \end{aligned}$$

which, after some simplifications, reduces to

$$0 = G^2 \frac{\mathbf{Z}^H \mathbf{X}}{\sigma_w^2} + G \left(\frac{\mathbf{X}^H \mathbf{X}}{\sigma_v^2} - \frac{\mathbf{Z}^H \mathbf{Z}}{\sigma_w^2} \right) - \frac{\mathbf{X}^H \mathbf{Z}}{\sigma_v^2}. \quad (5)$$

Equation (5) is quadratic in G and hence, there exist two extrema given by

$$G_{1,2} = \frac{-b \pm \sqrt{b^2 - 4ac}}{2a} \quad (6)$$

with

$$a = \frac{\mathbf{Z}^H \mathbf{X}}{\sigma_w^2}, \quad b = \frac{\mathbf{X}^H \mathbf{X}}{\sigma_v^2} - \frac{\mathbf{Z}^H \mathbf{Z}}{\sigma_w^2}, \quad \text{and} \quad c = -\frac{\mathbf{X}^H \mathbf{Z}}{\sigma_v^2}.$$

Unfortunately, it is not trivial to determine which of the two solutions maximizes (4). On the other hand, it is computationally cheap to calculate both \hat{G}_1 and \hat{G}_2 and then evaluate (4) in order to determine the solution.

Given the ML estimate \hat{G} , the MLE for the excitation signal is then [9]

$$\begin{aligned} \hat{\mathbf{U}} &= \left(\mathbf{H}^H \mathbf{C}^{-1} \mathbf{H} \right)^{-1} \mathbf{H}^H \mathbf{C}^{-1} \boldsymbol{\mathcal{X}} \Big|_{G=\hat{G}} \\ &= \left(\frac{1}{\sigma_v^2} + \frac{\hat{G} \hat{G}^*}{\sigma_w^2} \right)^{-1} \left(\frac{1}{\sigma_v^2} \mathbf{X} + \frac{1}{\sigma_w^2} \hat{G}^* \mathbf{Z} \right) \end{aligned} \quad (7)$$

The Cramér-Rao lower bound (CRB) and the asymptotic variance are given through the Fisher information matrix [9] which is

$$\begin{aligned} \mathcal{I}(\boldsymbol{\theta}) &= \begin{bmatrix} \mathbf{H}^H \mathbf{C}^{-1} \mathbf{H} & \mathbf{H}^H \mathbf{C}^{-1} \frac{\partial \mathbf{H}}{\partial G} \mathbf{U} \\ \mathbf{U}^H \left(\frac{\partial \mathbf{H}}{\partial G} \right)^H \mathbf{C}^{-1} \mathbf{H} & \mathbf{U}^H \left(\frac{\partial \mathbf{H}}{\partial G} \right)^H \mathbf{C}^{-1} \frac{\partial \mathbf{H}}{\partial G} \mathbf{U} \end{bmatrix} \\ &= \begin{bmatrix} \left(\frac{1}{\sigma_v^2} + GG^* \frac{1}{\sigma_w^2} \right) \mathbf{I}_M & \frac{1}{\sigma_w^2} G^* \mathbf{U} \\ \frac{1}{\sigma_w^2} G \mathbf{U}^H & \frac{1}{\sigma_w^2} \mathbf{U}^H \mathbf{U} \end{bmatrix}. \end{aligned}$$

Using block-wise inversion yields

$$\lim_{M \rightarrow \infty} \operatorname{cov}\{\hat{\boldsymbol{\theta}}\} = \mathcal{I}^{-1}(\boldsymbol{\theta}) = \begin{bmatrix} [\mathbf{C}_\theta]_{11} & [\mathbf{C}_\theta]_{12} \\ [\mathbf{C}_\theta]_{21} & [\mathbf{C}_\theta]_{22} \end{bmatrix} \quad (8)$$

with

$$\begin{aligned} [\mathbf{C}_\theta]_{11} &= \frac{\sigma_v^2 \sigma_w^2}{\sigma_w^2 + GG^* \sigma_v^2} \left(\mathbf{I}_M + \frac{\sigma_v^2}{\sigma_w^2} GG^* (\mathbf{U}^H \mathbf{U})^{-1} \mathbf{U} \mathbf{U}^H \right) \\ [\mathbf{C}_\theta]_{12} &= -\sigma_v^2 (\mathbf{U}^H \mathbf{U})^{-1} G^* \mathbf{U} \\ [\mathbf{C}_\theta]_{21} &= -\sigma_v^2 (\mathbf{U}^H \mathbf{U})^{-1} G \mathbf{U}^H \\ [\mathbf{C}_\theta]_{22} &= (\sigma_w^2 + GG^* \sigma_v^2) (\mathbf{U}^H \mathbf{U})^{-1} \end{aligned}$$

Finally, the complete non-parametric FRF $\hat{G}(\omega_l)$ is obtained from the input-output measurements by using the estimators (6)-(8) for each frequency bin ω_l individually.

III. SIMULATION

A. Estimator Properties

First, the estimator's performance is illustrated using Monte Carlo simulations. The Fourier transform yields independent coefficients for the input and output spectra and thus, it is enough to verify the estimator properties for a single coefficient only.

Since the estimator depends on the input and output noise properties, the effect of different signal to noise ratios (SNR) on the performance is analyzed first. The SNRs at the input and output are defined as

$$\operatorname{SNR}_I = 10 \log_{10} \left(\frac{\frac{1}{M} \mathbf{U}^H \mathbf{U}}{\sigma_v^2} \right)$$

and

$$\operatorname{SNR}_O = 10 \log_{10} \left(\frac{\frac{1}{M} \mathbf{Y}^H \mathbf{Y}}{\sigma_w^2} \right) = 10 \log_{10} \left(\frac{\frac{1}{M} GG^* \mathbf{U}^H \mathbf{U}}{\sigma_w^2} \right)$$

First, the input SNR is varied from 20 dB, 10 dB, 0 dB, to -10 dB, while keeping the output SNR constant at 20 dB. Then, the input SNR

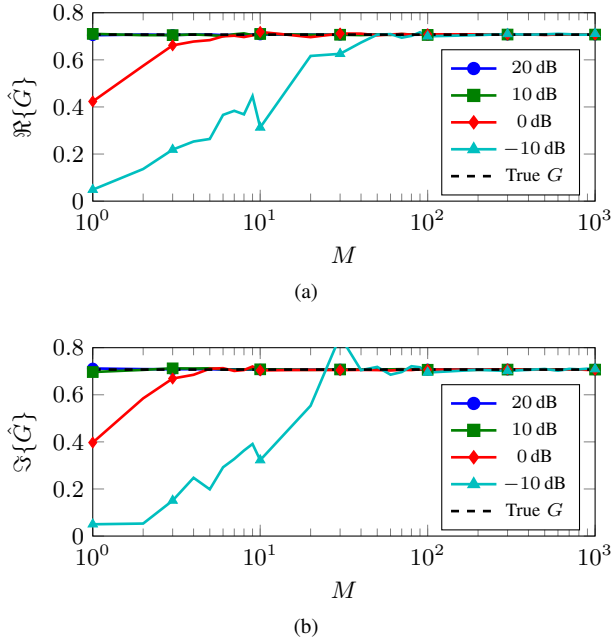


Fig. 2. Real (top) and imaginary parts (bottom) of the mean of the estimated \hat{G} for varying input SNR of the 1,000 Monte Carlo simulations.

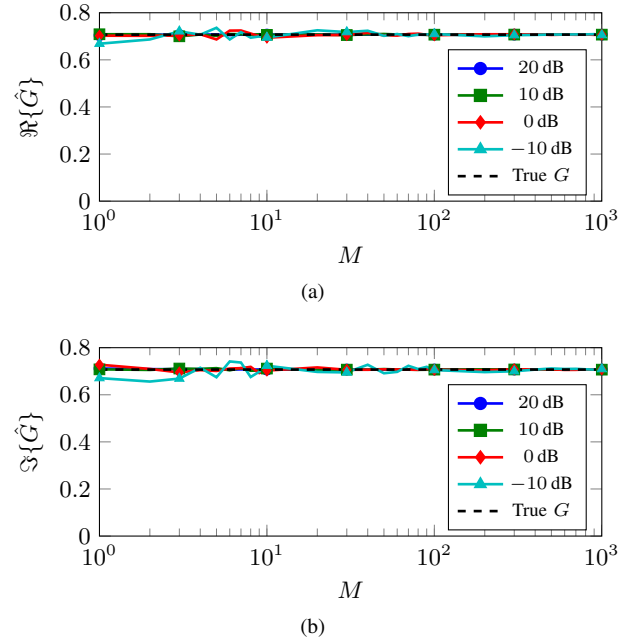


Fig. 4. Real (top) and imaginary parts (bottom) of the mean of the estimated \hat{G} for varying output SNR of the 1,000 Monte Carlo simulations.

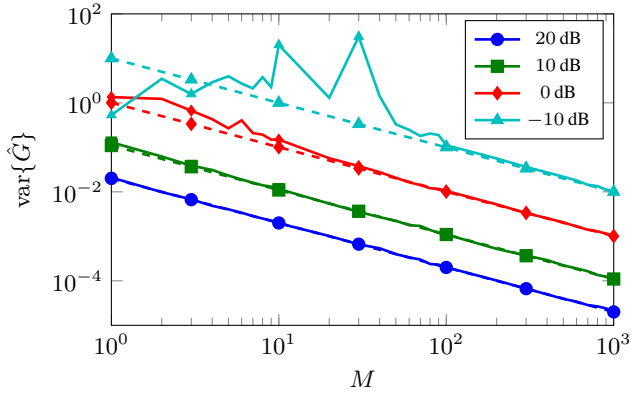


Fig. 3. Variance of the 1,000 Monte Carlo estimates for \hat{G} and CRB (dashed lines) for varying input SNR.

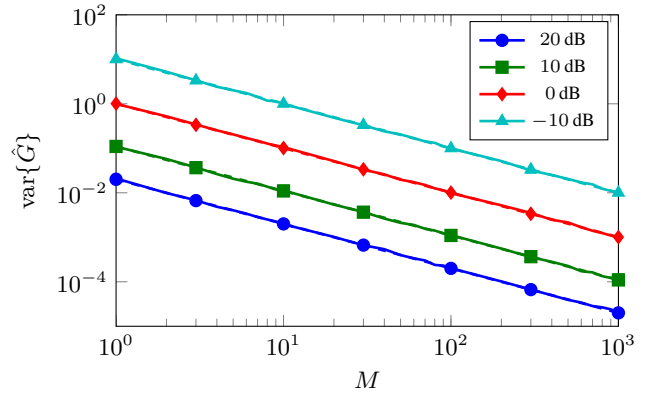


Fig. 5. Variance of the 1,000 Monte Carlo estimates for \hat{G} and CRB (dashed lines) for varying output SNR.

is kept constant at 20 dB and the output SNR varied from 20 dB, 10 dB, 0 dB, to -10 dB.

The input signal \mathbf{U} is chosen such that

$$\mathbf{U}^H \mathbf{U} = M$$

and the true value for G as

$$G = \frac{1}{\sqrt{2}}(1 + i)$$

so that the SNR is varied by varying the variances σ_v^2 and σ_w^2 . For each SNR combination, a total of 1,000 Monte Carlo simulations are performed and the results are averaged accordingly.

1) *Varying Input SNR*: The mean of the 1,000 Monte Carlo simulations where the input SNR was varied is shown in Fig. 2. As expected, the estimator converges to the true value (dashed black line). Even for an SNR as low as 0 dB, less than $M = 10$ experiments are required to obtain an unbiased estimate. For higher SNRs, the estimator converges even quicker and vice-versa for lower SNRs.

The fast convergence is also reflected in comparing the sample variance of the simulations to the CRB given by (8) shown in Fig. 3.

Again, for an SNR of 0 dB, the CRB is attained at around $M = 10$ experiments where higher SNRs guarantee that the CRB is attained almost immediately.

2) *Varying Output SNR*: Fig. 4 illustrates \hat{G} as a function of the number of experiments M for varying SNRs at the output. Clearly, the estimator is less sensitive to disturbances at the output since fast convergence is obtained even for an SNR of -10 dB. Similar to the previous case, less than $M = 10$ input-output pairs are required to obtain an unbiased estimate of the FRF coefficient.

Fig. 5 illustrates the sample variance of \hat{G} versus the CRB. As it can be seen from the graph, the CRB is attained immediately even for very small M and low SNRs. This in turn indicates that the proposed estimator essentially becomes efficient immediately under the given conditions.

B. Pendulum Example

Having verified the properties of the estimator in the previous section, it is now applied to a mass suspended from a moving pivot as illustrated in Fig. 6. This type of pendulum problem is encountered in

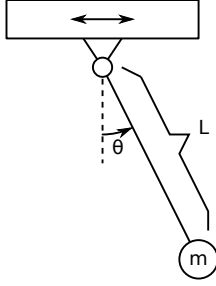


Fig. 6. Illustration of the pendulum suspended from a moving pivot.

TABLE I
SIMULATION PARAMETERS.

Parameter	Symbol	Value
Number of Experiments	M	10
Sampling Frequency	f_s	32 Hz
Number of Samples	N	1024
Excitation Location	t_0	5 s
Pulse Bandwidth	τ	0.25 s and 1 s
Input Measurement Noise	σ_v^2	1
Output Measurement Noise	σ_w^2	0.1
Load Mass	m	1 kg
Suspension Length	L	1 m
Friction Constant	b	1 kg m ² /s

many different applications such as cargo cranes in harbors, hauling loads using helicopters, or cable cars. The non-linear differential equation describing the system is given by

$$L\ddot{\theta} = -\frac{b}{mL}\dot{\theta} - g\sin(\theta) - u\cos(\theta). \quad (9)$$

In equation (9), m is the mass of the load, L is the length of the suspension wire, θ is the deflection angle of the pendulum, b is a friction coefficient in the pivot, $g = 9.81 \text{ m/s}^2$ is the gravitational acceleration, and u is the acceleration acting at the pivot.

In order to identify the linearized system around the equilibrium point $\theta = 0$, the system is excited by pulses of the form

$$u_m(t) = A_m \left(\frac{2}{\pi\tau^2} \right)^{1/2} e^{-\left(\frac{t-t_0}{\tau}\right)^2} \quad (10)$$

where t_0 is a time shift and τ controls the pulse bandwidth. The amplitude A_m was chosen randomly according to $A_m \sim \mathcal{U}[0.75, 1.25]$. Furthermore, note that we chose (10) such that

$$\|u_m(t)\|_2^2 = A_m.$$

This choice allows for easy adjustment of the mean input SNR through the input noise variance as

$$\mathbb{E}\{\text{SNR}_I\} = \mathbb{E}\left\{ \frac{\|u_m(t)\|_2^2}{\sigma_v^2} \right\} = \frac{\mathbb{E}\{\|u_m(t)\|_2^2\}}{\sigma_v^2} = \frac{\mathbb{E}\{A_m\}}{\sigma_v^2}.$$

The remaining parameters are chosen as listed in Table I. In order to illustrate different aspects of the method, we will compare two different experiments: one where we chose a narrow input pulse ($\tau = 0.25 \text{ s}$) which yields a high input bandwidth and one with a broader pulse ($\tau = 1 \text{ s}$) with a lower input bandwidth. Furthermore, we also compare the proposed estimator to the least squares estimator

$$\hat{G}_{LS}(\omega_l) = (\mathbf{X}^H \mathbf{X})^{-1} \mathbf{X}^H \mathbf{Z}. \quad (11)$$

Finally, we perform a total of 100 Monte Carlo simulations in order to analyze the average performance of the estimator.

Fig. 7 shows the estimated FRFs for the proposed maximum likelihood estimator and the least squares estimator when $\tau = 0.25 \text{ s}$. Also

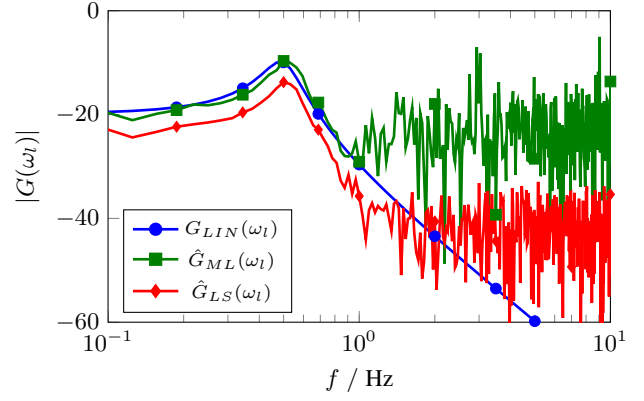


Fig. 7. Linearized and estimated non-parametric FRFs for a pendulum with moving pivot for $\tau = 0.25 \text{ s}$.

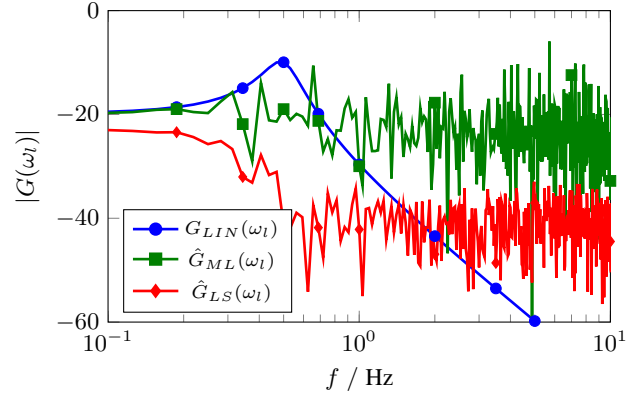


Fig. 8. Linearized and estimated non-parametric FRFs for a pendulum with moving pivot for $\tau = 1 \text{ s}$.

shown is the FRF of the linearized system around the equilibrium point $\theta = 0$ given by

$$G_{LIN} = -\frac{1}{s^2 + s\frac{b}{mL^2} + \frac{g}{L}}.$$

(Note that the linear approximation holds reasonably well for $|\theta| \leq 15^\circ$.) As it can be seen from Fig. 7, the maximum likelihood estimator proposed here is able to capture the dynamics of the considered system well up to around $f \approx 1 \text{ Hz}$. The least squares estimator does not perform as well and yields a biased estimate of the FRF. This behavior can readily be verified by looking at (11):

$$\begin{aligned} \mathbb{E}\{\hat{G}_{LS}(\omega_l)\} &= \mathbb{E}\{(\mathbf{X}^H \mathbf{X})^{-1} \mathbf{X}^H \mathbf{Z}\} \\ &= \mathbb{E}\{(\mathbf{X}^H \mathbf{X})^{-1}\} \mathbf{U}^H \mathbf{U} \mathbf{G} \\ &\quad + \mathbb{E}\{(\mathbf{X}^H \mathbf{X})^{-1} \mathbf{V}^H\} \mathbf{U} \mathbf{G} \\ &\neq \mathbf{G}. \end{aligned}$$

The same results but for $\tau = 1 \text{ s}$ are shown in Fig. 8. Clearly, in this case, none of the estimators is capable of reconstructing the frequency response function. This is, however, due to a poor choice of the excitation signal and not the estimator itself. Specifically, the excitation signal used in the second case does not cover all of the interesting dynamics of the system and hence, the information can not be extracted. This is also illustrated in Fig. 9 where the spectra of two excitation signals, one for each case, are shown. As it can be seen, the bandwidth of the second case ($\tau = 1 \text{ s}$) is much lower and does not excite the important dynamics around 0.5 Hz well enough. Clearly, this has to be taken into account when designing the experiment.

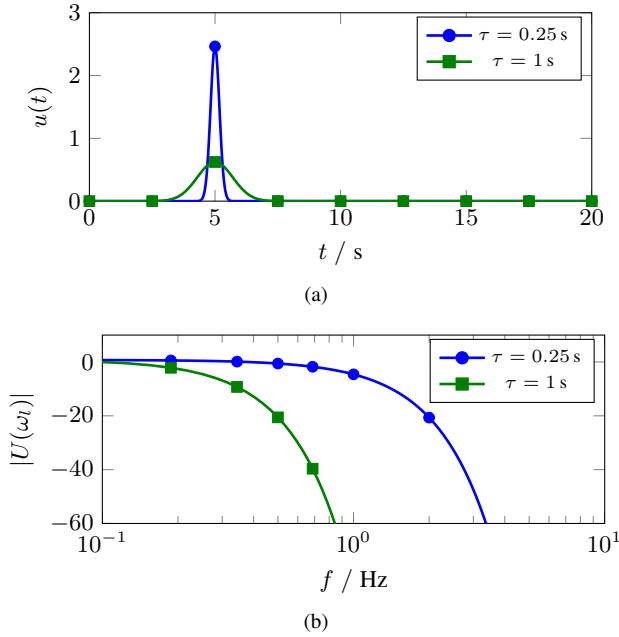


Fig. 9. Comparison of the excitation signals and their spectra. (a) Time-domain signals, (b) spectra.

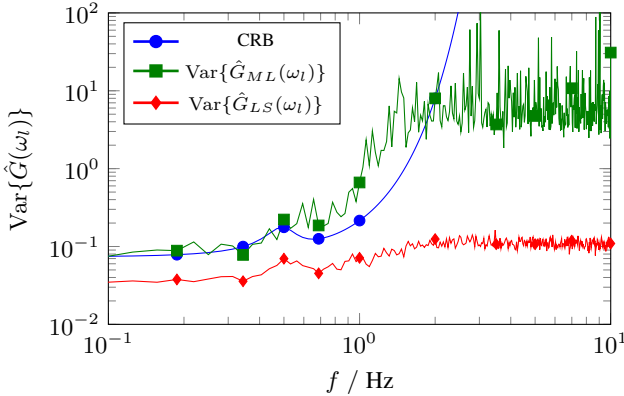


Fig. 10. Cramér-Rao lower bound together with the sample variances for the maximum likelihood and least squares estimators for $\tau = 0.25$ s.

Finally, the sample variance for $\hat{G}_{ML}(\omega_l)$ as well as $\hat{G}_{LS}(\omega_l)$ calculated using the 100 Monte Carlo simulations and the Cramér-Rao lower bound (CRB) are shown in Fig. 10 for $\tau = 0.25$ s and Fig. 11 for $\tau = 1$ s. For $\tau = 0.25$ s (Fig. 10), it can be seen that the variance for the proposed estimator closely follows the CRB for frequencies where a reasonable SNR (as established in Section III-A) is obtained. The performance then degrades, once the excitation signal becomes weaker (lower SNR for these frequencies). For the least squares estimator, we observe that the sample variance is below the CRB for all frequencies. This is not surprising since it is not uncommon for biased estimators to have variances below the CRB [9]. In the second case ($\tau = 1$ s, Fig. 11), neither of the estimators achieves the CRB. The reason for the maximum likelihood estimator not attaining the CRB is again the poor design of the input signal which yields a too low SNR even in the range of excited frequencies. As in the case for $\tau = 0.25$ s, the least squares estimator has a sample variance lower than the CRB due to its biasedness (see Fig. 8).

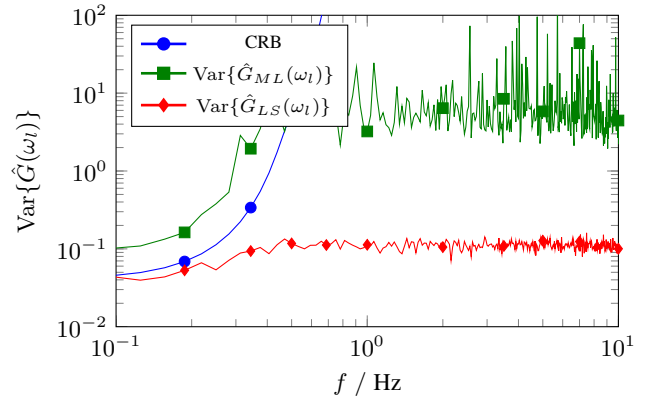


Fig. 11. Cramér-Rao lower bound together with the sample variances for the maximum likelihood and least squares estimators for $\tau = 1$ s.

IV. CONCLUSION

This paper introduced the closed-form maximum likelihood estimator for the non-parametric frequency response function in an error-in-variables setting. The estimator is based on repeated, possibly non-reproducible measurements as they may arise in a variety of different applications.

It has been shown that the estimator converges to the true value and attains the Cramér-Rao lower bound quickly. In practice, about 10 measurements at input and output signal-to-noise ratios of 0 dB and 20 dB, respectively, are necessary. Furthermore, if the input can be measured reasonably well, an output SNR of only -10 dB yields a consistent estimate when using 10 measurements. Comparison between the proposed MLE and the least-squares estimator showed that the latter is biased and hence, the MLE is to be preferred.

REFERENCES

- [1] R. Pintelon and J. Schoukens, *System Identification: A Frequency Domain Approach*. Piscataway, NJ, USA: Wiley-IEEE Press, 2001.
- [2] L. Ljung, *System Identification: Theory for the User*. Upper Saddle River, NJ, USA: Prentice Hall, 1997.
- [3] J. Schoukens, R. Pintelon, E. van der Ouderaa, and J. Renneboog, "Survey of excitation signals for FFT based signal analyzers," *Instrumentation and Measurement, IEEE Transactions on*, vol. 37, no. 3, pp. 342–352, 1988.
- [4] J. Schoukens, R. Pintelon, G. Vandersteen, and P. Guillaume, "Frequency-domain system identification using non-parametric noise models estimated from a small number of data sets," *Automatica*, vol. 33, no. 6, pp. 1073–1086, 1997.
- [5] T. Söderström, K. Mahata, and U. Soverini, "Identification of dynamic errors-in-variables models: Approaches based on two-dimensional ARMA modeling of the data," *Automatica*, vol. 39, no. 5, pp. 929–935, 2003.
- [6] T. Söderström, "Errors-in-variables methods in system identification," *Automatica*, vol. 43, no. 6, pp. 939–958, 2007.
- [7] J. W. Gillard, "An historical overview of linear regression with errors in both variables," Cardiff University, Tech. Rep., 2006.
- [8] E. Zhang, R. Pintelon, and J. Schoukens, "Errors-in-variables identification of dynamic systems excited by arbitrary non-white input," *Automatica*, vol. 49, no. 10, pp. 3032–3041, 2013.
- [9] S. M. Kay, *Fundamentals of Statistical Signal Processing: Estimation Theory*. Upper Saddle River, NJ, USA: Prentice Hall, 1993.
- [10] A. Van Den Bos, "Complex gradient and Hessian," *Vision, Image and Signal Processing, IEE Proceedings on*, vol. 141, no. 6, pp. 380–383, 1994.